Sensors and Materials, Vol. 36, No. 4 (2024) 1645–1659
MYU Tokyo

S & M 3624

Almost Finite-time Synchronization of Coronary Artery Systems via Adaptive Fractional-powered-integral-type Sliding Mode Control Method

Hao Hong, Linuo Lai, Chi-Hsin Yang,* and Kun-Chieh Wang

School of Mechanical and Electric Engineering, Sanming University, Sanming 365004, Fujian Province, China

(Received October 20, 2023; accepted April 4, 2024)

Keywords: coronary artery system, almost finite-time synchronization, integral-type SMC

When treating a vasospasm brought on by a malfunctioning coronary artery system (CAS), the goal is to enhance the physiology of the CAS by synchronizing its dynamic behavior with that of a healthy CAS, according to the perspective of cardiac medicine. This treatment is supported by a sophisticated automated detection and visualization system for the identification of a diseased CAS. For the biomathematical model of a CAS, we provide, in this study, a novel fractional-powered-integral-type finite-time-convergent sliding mode (FFSM), which is composed of the fractional-powered and integral terms of state variables. To achieve almost finite-time synchronization between two CASs, an adaptive sliding mode (SM) control approach in terms of the stated FFSM is introduced. Upon the implementation of the devised control, a special form of stability is demonstrated. That is, because of a feature of the model for a CAS, the two error states are stabilized sequentially on the sliding surface, resulting in an almost finite-time stability. The nonlinear dynamical consequences of the synchronized error system can be countered by the adaptive FFSM control scheme, which consists of three online updated gains with the principles of adaptation. To demonstrate the validity of the current scheme, numerical experiments are carried out.

1. Introduction

It is commonly known in cardiac physiology that the coronary artery system (CAS) transports vital materials to the heart, including blood, nutrients, and oxygen. Several clinical cases have led cardiologists to conclude that people with a high risk of sudden cardiac death have a disturbed physiological status and irregular heartbeats.(1) One example is vascular spasm, which is caused by the blood vessels operating incoherently. The complexity of heart action rises with a change in vessel diameter. The provoked coronary artery vasospasm occurs when the coronary artery vessels enter states of chaos.(2) Many works on chaos in a CAS have been reported because of its importance.(3–8)

The Melnikov approach has been used to build and examine two basic types of biomathematical models for muscle blood arteries, namely, N-type and S-type, in order to

*Corresponding author: e-mail: 20190207@fjsmu.edu.cn
https://doi.org/10.18494/SAM4727

ISSN 0914-4935 © MYU K.K.

explore the chaos of a CAS.[3] The dynamics of the variations in blood pressure and the coronary artery vessel inner radius in a CAS are described using mathematical models. In previous works, the N-type CAS's complex behaviors were examined in relation to two different types of system parameter sets.[4,5] Hardware was also created by circuit implementation to mimic a CAS's nonlinear dynamics. Additionally, the dynamics of fractional-order CASs were presented and introduced.[7,8]

For the detection of a diseased CAS, an automatic detection and visualization system that applies optical frequency domain images was built.[9] The developed system is associated with a deep learning network and can recognize the medical types of CAS and help to control the diseased CAS. From a medical perspective, the diseased CAS becomes capable of multiple periodic movements through medical therapy, which improves the pathological change of the diseased CAS and treats the vasospasm caused by a CAS in a chaotic state.[10] From the perspective of control systems, treatment for cardiovascular disorders is viewed as applying an appropriate control input to a diseased CAS in a chaotic status to force it to synchronize with a healthy CAS that is functioning in multi-periodic movements. Chaotic synchronization has been a hot research topic owing to its potential for use in science and technology, including MEMS, circuit systems, image encryption, secure communication, nervous systems, and nervous system imaging.[11–16] The primary objective of chaotic synchronization is to apply the appropriate control technique to achieve the same behavior across the driving and response systems.

The SM control method for curbing the chaos of a CAS is based on the created biomathematical model and was reported in Ref. 4 to be the solution for solving it. Numerous previous studies regarding the chaotic synchronization of CASs have also been documented. In 2013,[5] fuzzy logic control was used to achieve synchronization associated with the differential transformed technique. To prevent chattering phenomena, the high-order SM adaptive control approach was created in 2015.[17] In 2017, Wu *et al*. created the self-tuning terminal SMC[18] and Wu *et al*. employed the state feedback control system.[10]

Furthermore, there have been numerous previous papers on the hot topic of the chaotic synchronization of CASs with the time-delay phenomenon, including those on observer-based control schemes,[19,20] the synchronized control scheme with input saturation,[21] the adaptive fuzzy control scheme,[22] the H∞ synchronization technique,[23] and the finite-time control considering input delay.[2] Recently, for a CAS, output feedback control created by bilinear matrix inequality (BMI) for synchronizing pathological differences and chaos suppression by second-order SM techniques have been described.[24,25] In this study, in order to synchronize the drive (healthy) and response (diseased) CASs in almost finite time, we devised a novel adaptive fractional-powered-integral-type finite-time-convergent sliding mode control (FFSMC) approach referring to the work in prior studies.[4,5,14,18] The features and innovations of our study are summarized as follows.

(1) The research topic of cardiac pathologic therapy is transformed into a control design problem of nonlinear systems from the viewpoint of the control system using the biomathematical model of the CAS.
(2) The chaos of CASs was primarily studied with two separate parameter sets incorporated in the system in previous research.[4,5] It is assumed that in the control problem of

synchronization between two chaotic CASs, the two chaotic CASs have the same parameter configuration.[4–6,10,17,18] The more realistic supposition that each of the drive (healthy) and response (diseased) CASs has an individual set of system characteristics is used in this work to explain synchronization.

(3) A novel FFSM is offered to address the chaotic synchronization control issue for two CASs. The fractional-powered and integral terms of state variables make up the described FFSM, which has a unique stable feature. That is, the stability of an error state in finite time first occurs on the sliding surface. The exponential stability of the other state is then brought about in the following way. A comprehensive piece of evidence of stability is supplied.

(4) To achieve an almost finite-time synchronization, an adaptive FFSMC system is designed for two CASs. The equivalent control of the inserted SMC directly cancelled the nonlinear dynamics in previous investigations,[4,5,17] including cubic items and external excitation. In contrast to previous research, our adaptive FFSMC scheme can counteract the nonlinear dynamics of the synchronized error dynamical system. It consists of three updated feedback gains with the stated principles of adaptation.

In Sect. 2 of this work, we present the challenge in controlling the synchronization of two CASs. The procedures involved in developing the adaptive FFSMC approach are presented in Sect. 3. The whole close-loop control system's stability is also demonstrated. In Sect. 4, numerical experiments to validate the suggested control mechanism are described. Lastly, a few closing thoughts are expressed.

2. Formulation of Controlling Synchronization for Two CASs

The following defines the biomathematical system of a CAS:[4,5]

$$\begin{cases} \dot{x} = -Bx - Cy, \\ \dot{y} = -\lambda(1+B)x - \lambda(1+C)y + \lambda x^3 + E\cos(\omega t). \end{cases} \tag{1}$$

Here, t is the dimensionless time and the dimensionless state variables x, y stand for the differences in the inner radius of the vessel and blood pressure, respectively. The parameters B, C, and λ of the system primarily govern the dynamic behaviors of the CAS. $E\cos(\omega t)$ is the external excitation for the blood vessels.

The chaos of a CAS versus the variation of $E \in [0.1, 20]$ was examined in Ref. 5, where the system parameters were set to $B = 0.15$, $C = -0.17$, and $\lambda = -0.65$ with $\omega = 1.0$. We infer that when $E \in [0.3, 0.6)$ and $E \in [4.5, 5.9)$, the CAS generates chaotic motions. On the other hand, it exhibits multi-periodic movements. Figure 1 shows the phase picture of Eq. (1) for $\lambda = -0.65$, $E = 0.5$ in the absence of control input. It represents the breakdown of the CAS into anarchy and presents it as the main ill case thereafter. When the CAS has multi-periodic motion with $\lambda = -0.5$, $E = 0.6$,[4] the driving system or healthy CAS is constructed. The phase portrait is displayed in Fig. 2.

The control problem for synchronization between the diseased and healthy CASs is taken into consideration. Using the additional defined state variables x_d, y_d and the system

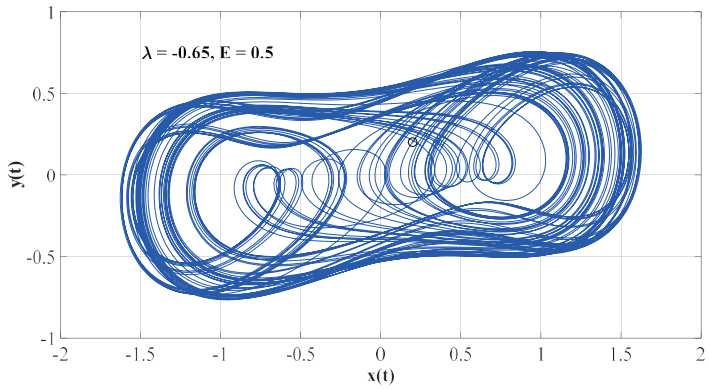

Fig. 1. (Color online) Phase portrait of the primary diseased CAS (in chaos).

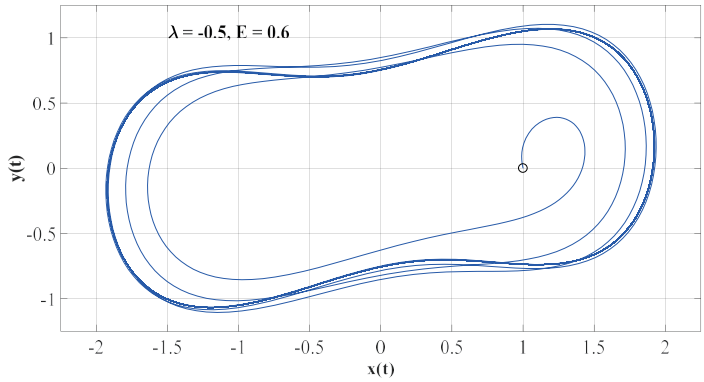

Fig. 2. (Color online) Phase portrait of the healthy CAS (in multi-periodic motion).

characteristics in Fig. 2, the healthy CAS is defined in Eq. (1) for synchronization. With the following additions, the primary diseased CAS shown in Fig. 1 serves as a model for the reaction

$$\begin{cases} \dot{x}_r = -Bx_r - Cy_r, \\ \dot{y}_r = -\lambda_r(1+B)x_r - \lambda_r(1+C)y_r + \lambda_r x_r^3 \\ \qquad + E_r\cos((\omega+\delta)t) + \Delta(x_r, y_r) + D(t) + \phi(t). \end{cases} \tag{2}$$

The state variables are denoted by x_r and y_r. The system parameters λ, E applied to the healthy CAS in Eq. (1) are different from the system parameters λ_r, E_r. Additionally, in contrast to earlier research,[4–6,10,17,18] an uncertainty δ also disturbs the radial frequency ω of the external stimulation, affecting the blood vessels. The unmodeled system dynamics are represented by $\Delta(x_r, y_r)$ and the additional external disturbance is represented by $D(t)$. The dosage of medication used to treat cardiac problems is determined using the associated control input $\phi(t)$. To bring the state variables of the diseased CAS in Eq. (2) and the healthy one in Eq.

(1) into synchrony, or $\lim_{t\to\infty} x_r(t) \to x_d(t), \lim_{t\to\infty} y_r(t) \to y_d(t)$, for any given set of beginning circumstances, the control problem is handled by adding the proper control scheme $\phi(t)$.

Assumption

Both the extra external disturbance $D(t)$ and the unmodeled system dynamics $\Delta(x_r, y_r)$ are bounded and unknown. It is presumed that

$$0 < |\Delta(x_r, y_r)| < N_1,\ 0 < |D(t)| < N_2, \tag{3}$$

where N_1, N_2 are uncertain constants.

The synchronized error state between the healthy and diseased CASs in Eqs. (1) and (2) for achieving control is

$$\varepsilon_x(t) = x_r(t) - x_d(t),\ \varepsilon_y(t) = y_r(t) - y_d(t). \tag{4}$$

The governing equation of error states is Eq. (5), which takes the derivative of Eq. (4) versus t.

$$\begin{cases} \dot{\varepsilon}_x = -B\varepsilon_x - C\varepsilon_y \\ \dot{\varepsilon}_y = \lambda_r(f_1(x_r, x_d) - 1 - B)\varepsilon_x - \lambda_r(1 + C)\varepsilon_y + (\lambda - \lambda_r)f_2(x_d, y_d) \\ \qquad + E_r\cos((\omega + \delta)t) - E\cos(\omega t) + \Delta(x_r, y_r) + D(t) + \phi(t) \end{cases} \tag{5}$$

The healthy and diseased CASs exhibit chaotic or multi-period motional phase profiles, which results in the boundedness of functions $f_1(x_r, x_d) = x_r^2 + x_r x_d + x_d^2$ and $f_1(x_r, x_d) = x_r^2 + x_r x_d + x_d^2$. $f_1(x_r, x_d)$ and $f_2(x_r, x_d)$ represent the variable gain of $\varepsilon_x(t)$ and another additional disturbance, respectively, in the control development process. They are

$$0 < \left|f_1(x_r, x_d)\right| < M_1, < \left|f_2(x_d, y_d)\right| < M_2, \tag{6}$$

where M_1, M_2 are uncertain constants. The problem at this stage is equal to the control $\phi(t)$ that is intended to stabilize the dynamic system in Eq. (5).

Definition 1

Equations (1) and (2) achieve synchronization between the healthy and diseased CASs, which is equal to $\lim_{t\to\infty}\left|\varepsilon_x(t)\right| \to 0$ and $\lim_{t\to\infty}\left|\varepsilon_y(t)\right| \to 0$.

Achieving proper control $\phi(t)$ as defined in Definition 1 to stabilize the error states in Eq. (5) is crucial for synchronizing the healthy and diseased CASs.

3. Proceeding Adaptive Integral-type Sliding Mode Control

For system Eq. (5), an adaptive SMC approach is developed to provide synchronization between two CASs in nearly finite time, on the basis of the newly introduced FFSM. Later, the

stability of FFSM is clarified. The stability of FFSM acts such that it first induces the stabilization of an error state in finite time. Next, on the sliding surface, the other error state's exponential stability is brought about as follows. Prior to delving into the primary findings, the practical lemma concerning finite-time stability is discussed.

Lemma:[26] For the first-order dynamical system,

$$\sigma(t) = \dot{\theta}(t) + a\theta(t) + b\left[\theta(t)\right]^{n/m} = 0, \tag{7}$$

where a, b are positive real parameters and $m > 0$, $n > 0$ are odd integers satisfying $0 < n/m < 1$. It is guaranteed that $\sigma(t) = 0$ with the initial condition $\theta_0 \neq 0$ will remain stable in finite time. Additionally, $\theta(t)$ is stabilized to the origin at the specified time calculated as

$$T_s = \frac{m}{a(m-n)} \ln\left[\frac{a}{b}\left(\theta_0\right)^{(m-n)/m} + 1\right] > 0, \tag{8}$$

and $\theta(t) = 0$ holds after $\forall t \geq T_s > 0$.

Remark 1

The faster terminal sliding surface $\sigma(t) = 0$ that is defined and discussed in Ref. 26 is that of Eq. (7). The stabilized finite time is calculated using Eq. (8), where the origin is a terminal attractor. The details of the proof are not included here, but can be found in Ref. 26.

The planned procedure of the adaptive FFSMC scheme consists of two primary parts. The novel FFSM $s(t)$ is first defined, including its stability. Second, despite both internal and external disturbances, an adaptive control system based on the stated FFSM with adaptation criteria is presented to obtain the error states that can reach and stay on the phase plane's sliding surface $s(t) = 0$.

Definition 2

The innovative FFSM $s(t)$ is composed of the integral and fractional-powered terms of the state variables:

$$s(t) = [\varepsilon_y(t)]^{p/q} + \alpha \int_{\tau=0}^{t} [\varepsilon_y(\tau)]^{p/q} d\tau + \beta \left[\varepsilon_x(t) + B \int_{\tau=0}^{t} \varepsilon_x(\tau) d\tau \right], \tag{9}$$

where $\alpha, \beta > 0$ and $p > 0$, $q > 0$ are odd integers with $1 < p/q < 2$.

The stability on the sliding surface $s(t) = 0$ is covered in more detail later. To ensure the finite-time stability of the innovative FFSM in Eq. (9), the following Theorem 1 is the given criterion. $s(t) = 0$ with variety sets α, β is depicted in Fig. 3.

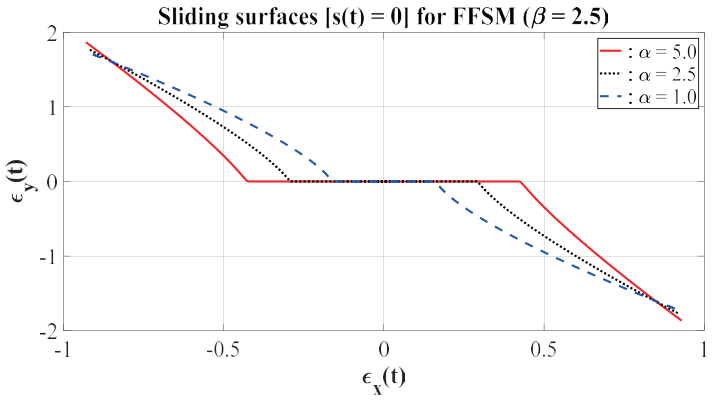

Fig. 3. (Color online) Sliding surface $s(t) = 0$ for FFSM.

Theorem 1

When $s(t) = 0$ and $\dot{s}(t) = 0$, the global finite-time stability of the synchronized error state $\varepsilon_y(t)$ is ensured for the FFSM $s(t)$ specified in Eq. (9). $\varepsilon_y(t)$ first tends to the origin [$\varepsilon_y(t) = 0$] during the finite time interval specified by

$$t_s = \frac{p}{\alpha(p-q)} \ln\left(\frac{\alpha}{|C|\beta} \left[\varepsilon_y(t_0)) \right]^{(p-q)/q} + 1 \right) + t_0, \tag{10}$$

where $t = t_0 > 0$ is the moment at which the state trajectory of $\varepsilon_y(t)$, $\varepsilon_y(t)$ reaches $s(t) = 0$ in the phase plane. Then, for $\forall t \geq t_s > 0$, $\varepsilon_y(t)$ remains at the origin. Following that, the state $\varepsilon_x(t)$ experiences exponential stabilization as follows.

Proof

$\dot{s}(t) = 0$ is satisfied when it reaches $s(t) = 0$ and remains there. The following equation governing the dynamical system of FFSM is obtained by substituting the first equation in Eq. (5) with $\dot{s}(t) = 0$:

$$\begin{aligned} &\dot{s}(t) = \frac{p}{q}\left[\varepsilon_y(t) \right]^{p/q-1} \dot{\varepsilon}_y(t) + \alpha\left[\varepsilon_y(t) \right]^{p/q} + \beta\left[\dot{\varepsilon}_x(t) + B\varepsilon_x(t) \right] = 0 \\ &\Rightarrow \frac{d\varepsilon_y(t)}{dt} + \frac{\alpha q}{p}\varepsilon_y(t) + \frac{-C\beta q}{p}\left[\varepsilon_y(t) \right]^{2-p/q} = 0. \end{aligned} \tag{11}$$

Here, $0 < 2 - p/q < 1$ for $1 < p/q < 2$. The initial condition of Eq. (11) is represented as $\varepsilon_y(t_0) \neq 0$. $t_0 > 0$ is the time spent to change $\varepsilon_x(t)$, $\varepsilon_y(t)$ from $\varepsilon_x(t_0)$, $\varepsilon_y(t_0)$ to $s(t) = 0$.

Applying the Lemma and setting up the necessary parameters for $n/m = 2 - p/q$, $a = \alpha q/p$, and $b = -C\beta q/p$ result in the assurance that $\varepsilon_y(t)$ is finite-time stable. Equation (10) yields the finite time t_s, which should go from $\varepsilon_y(t_0) \neq 0$ to $\varepsilon_y(t_s) = 0$ because of Eq. (8). Additionally, $\varepsilon_y(t) = 0$ and $\forall t \geq t_s > 0$ continuously. Following that, it is evident that the exponential stability of $\varepsilon_x(t)$ under

$\varepsilon_y(t) = 0$, $\forall t \geq t_s > 0$, is unquestionably guaranteed for $\varepsilon_y(t_s) \neq 0$. Specifically,

$$\dot{\varepsilon}_x(t) + B\varepsilon_x(t) = 0 \Rightarrow \varepsilon_x(t) = \varepsilon_x(t_s)\exp(-Bt),\ \ \forall t \geq t_s > 0,\ \ B > 0. \tag{12}$$

Thus, this proves Theorem 1.

As Theorem 2, the adaptive FFSMC with the adaptation rules based on FFSM in Eq. (9) is introduced. It can guarantee that, when confronted with system uncertainty and an external disturbance, the state trajectory of Eq. (5) will reach and maintain itself on the sliding surface $s(t) = 0$ and $\dot{s}(t) = 0$.

Theorem 2

If $\phi(\tau) = \phi_{eq}(\tau) + \phi_{sw}(\tau)$ is taken as the control scheme,

$$\begin{aligned} \phi_{eq}(t) &= \frac{C\beta q}{p}\left[\varepsilon_y(t)\right]^{2-p/q}, \\ \phi_{sw}(t) &= -\left[K_0(t) + K_1(t)\left|\varepsilon_x(t)\right| + K_2(t)\left|\varepsilon_y(t)\right|\right]\cdot \mathrm{sign}(s(t)). \end{aligned} \tag{13}$$

The state variables $\varepsilon_x(t)$, $\varepsilon_y(t)$ of system Eq. (5) will attain and persist on $s(t) = 0$ for dynamical system Eq. (5), where $s(t)$ is FFSM in Eq. (9) and the sign(•) is the sign function. According to the following adaptation principles, $K_i(t)$, $i = 0, 1, 2$ represent updated gains.

$$\begin{aligned} \dot{K}_0(t) &= \gamma_0\left|\varepsilon_y(t)\right|^{(p/q)-1}\left|s(t)\right|, \quad K_o(0) = 0, \quad \gamma_0 > 0 \\ \dot{K}_1(t) &= \gamma_1\left|\varepsilon_x(t)\right|\left|\varepsilon_y(t)\right|^{(p/q)-1}\left|s(t)\right|, \quad K_1(0) = 0, \quad \gamma_1 > 0 \\ \dot{K}_2(t) &= \gamma_2\left|\varepsilon_y(t)\right|^{(p/q)}\left|s(t)\right|, \quad K_2(0) = 0, \quad \gamma_2 > 0 \end{aligned} \tag{14}$$

$\varepsilon_y(t) \rightarrow 0$ in finite time and the exponential stabilization of $\varepsilon_x(t)$ then occurs after that point. Finally, CAS systems Eqs. (1) and (2) have attained an almost finite-time synchronization.

Proof

The choice of the positive Lyapunov function is made by

$$L(t) = \frac{1}{2}s^2(t) + \sum_{i=0}^{2}\frac{p}{2q\gamma_i}(K_i(t) - g_i)^2 \geq 0, \tag{15}$$

where $g_i > 0$, $i = 0, 1, 2$ is satisfied.

$$\begin{aligned} g_0 &> \left(\left|\lambda\right| + \left|\lambda_r\right|\right)M_2 + E_r + E + N_1 + N_2, \\ g_1 &> \left|\lambda_r\right|\left(M_1 + 1 + B\right) + \alpha, \\ g_2 &> \left|\lambda_r\right|\left(1 + \left|C\right|\right). \end{aligned} \tag{16}$$

The defined SM in Eq. (9), the adaptive FFSMC scheme in Eqs. (13) and (14), and the derivative of Eq. (15) vs t associated with the solutions of Eq. (5) yield the following.

$$\begin{aligned}
\dot{L}(t) &= s(t)\dot{s}(t) + \sum_{i=0}^{2} \frac{p}{q\gamma_i}(K_i(t) - g_i)\dot{K}_i(t) \\
&= s\left[\frac{p}{q}\left[\varepsilon_y\right]^{p/q-1}\dot{\varepsilon}_y + \alpha\left[\varepsilon_y\right]^{p/q} + \beta\left(\dot{\varepsilon}_x + B\varepsilon_y\right)\right] + \frac{p}{q}\sum_{i=0}^{2}\frac{K_i(t) - g_i}{\gamma_i}\dot{K}_i(t) \\
\Rightarrow \dot{L}(t) &= s\frac{p}{q}\left[\varepsilon_y\right]^{p/q-1}\cdot\left[\left[\lambda_r\left(f_1 - 1 - B\right) + \alpha\right]\varepsilon_x - \lambda_r\left(1 + C\right)\varepsilon_y\right. \\
&\quad + (\lambda - \lambda_r)f_2 + E_r\cos((\omega + \delta)t) - E\cos(\omega t) + \Delta + D \\
&\quad \left. - \left(K_0(t) + K_1(t)\left|\varepsilon_x\right| + K_2(\tau)\left|\varepsilon_y\right|\right)\cdot\mathrm{sign}(s)\right] \\
&\quad + \frac{p}{q}\sum_{i=0}^{2}\frac{K_i(t) - g_i}{\gamma_i}\dot{K}_i(t),
\end{aligned} \tag{17}$$

$$\begin{aligned}
\Rightarrow \dot{L}(t) &\le \frac{p}{q}\left|\varepsilon_y\right|^{p/q-1}\left|s\right|\cdot\left[-\left(g_0 - [\left|\lambda\right| + \left|\lambda_r\right|]M_2 - E_r - E - N_1 - N_2\right)\right. \\
&\quad \left. -\left(g_1 - \left[\left|\lambda_r\right|\left(M_1 + 1 + B\right) + \alpha\right]\right)\left|\varepsilon_x\right| - \left(g_2 - \left|\lambda_r\right|[1 + \left|C\right|]\right)\left|\varepsilon_y\right|\right] < 0.
\end{aligned} \tag{18}$$

The function $L(t)$ is a decreasing function vs t and is positive definite, as determined by Eqs. (15) and (18). It results in the global asymptotic stability of the equilibriums ($s = 0$, $K_i(t) = g_i$, $i = 0, 1, 2$). Furthermore, the implementation of the adaptive FFSMC scheme described by Eqs. (13) and (14) leads to the asymptotic convergence of $\varepsilon_x(t)$, $\varepsilon_y(t)$ in system Eq. (5) on $s(t) = 0$ and $\dot{s}(t) = 0$.

First, $\varepsilon_y(t)$ is stabilized at a finite time t_s on $s(t) = 0$, where t_s is given by Eq. (10). Subsequently, $\varepsilon_x(t)$ is then exponentially stabilized in the sequel, in accordance with Theorem 1. The so-called almost finite-time synchronization between the two CAS systems Eqs. (1) and (2) is achieved because $\varepsilon_y(t)$ is stabilized in finite time, and the exponential stabilization of $\varepsilon_x(t)$ occurs in sequence. Thus, this proves Theorem 2.

Remark 2

In Eq. (13), it is shown that $\varepsilon_x(t)$ in Eq. (5) is countered without nonlinear cancellation. This is significantly different from the earlier works.[4,5,17]

Remark 3

In Eq. (13), the control input is discontinuous. $\tanh(s/\sigma)$ modifies the sign function in Eq. (13) to reduce the chattering control signal. The numerical experiments use the amply modest value of $\sigma = 10^{-4}$, as described below.

4. Numerical Experiments and Discussion

In this section, the simulation program and execution for validating the proposed adaptive FFSMC system are described. The application is constructed and coded using the MATLAB-SIMULINK package. The software's built-in Runge–Kutta ode45 solver is used. Numerical integration is chosen with a tolerance of 10^{-8} and a variable step length.

The accompanying Table 1 provides an overview of the parameters used in the numerical experiments.

Next, the simulating scenes are developed to carry out the numerical experiments. The drive and response CASs without control input are operated separately from the initial conditions at $t = 0$ prior to the implementation of control. At $t = 15$ in two scenarios, the control input of the response CAS is turned on to start synchronization.

Figure 4 shows the phase pictures of $s(t)$ vs $\varepsilon_x(t)$ and $\varepsilon_y(t)$ for the first numerical experiment using $\alpha = 2.5$, $\gamma_0 = 15$, $\gamma_1 = 8$, and $\gamma_2 = 30$. The following shows that $\varepsilon_y(t)$ tends to the origin and that $s(t) = 0$ first converges to zero. In the sequel, $\varepsilon_x(t)$ is stabilized with $s(t) = 0$ and $\varepsilon_y(t) \to 0$. The FFSM property mentioned in Theorem 1 is confirmed. The time histories of $\varepsilon_x(t)$ and $\varepsilon_y(t)$ are shown in Fig. 5. It is seen that $\varepsilon_y(t)$ approaches zero faster than $\varepsilon_x(t)$. However, the long-term convergence of $\varepsilon_x(t) \to 0$ is unacceptable for controlled synchronization.

Table 1
Parameters for coding.

Name of parameter	Given values
Initial conditions	$(x_d, y_d) = (1.0, 0)$, $(x_r, y_r) = (0.2.\ 0.2)$
CAS parameters (common)	$\omega = 1.0$, $B = 0.15$, $C = -1.7$
Healthy (drive) CAS parameters	$\lambda = -0.5$, $E = 0.6$
Diseased (response) CAS parameters	$\lambda_r = -0.65$, $E_r = 0.5$, $\delta = 0.01$
Unmodeled dynamics	$\Delta(x_r, y_r) = 1.0 \cdot \sin(x_r)\cos(y_r)$
Other external disturbance	$D(t) = 0.25 \cdot \cos(2\omega t)$
Design parameters	$p = 13$, $q = 9$, $\beta = 2.5$

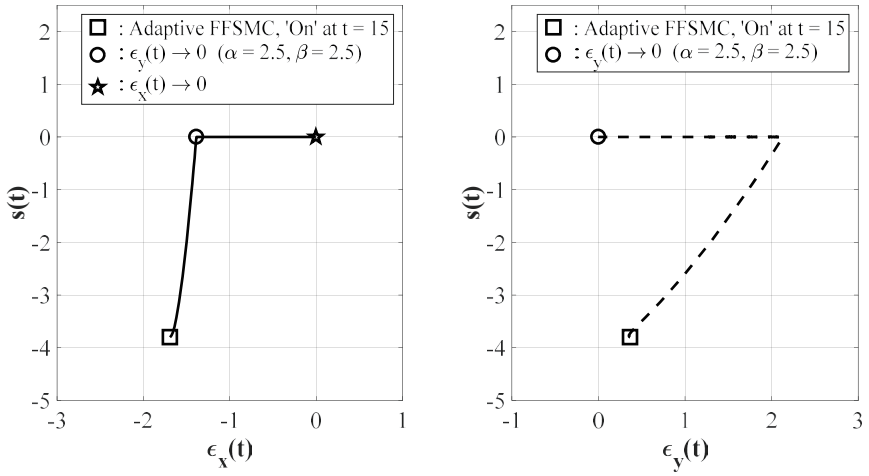

Fig. 4. Phase portraits of $s(t)$ versus $\varepsilon_x(t)$ and $\varepsilon_y(t)$.

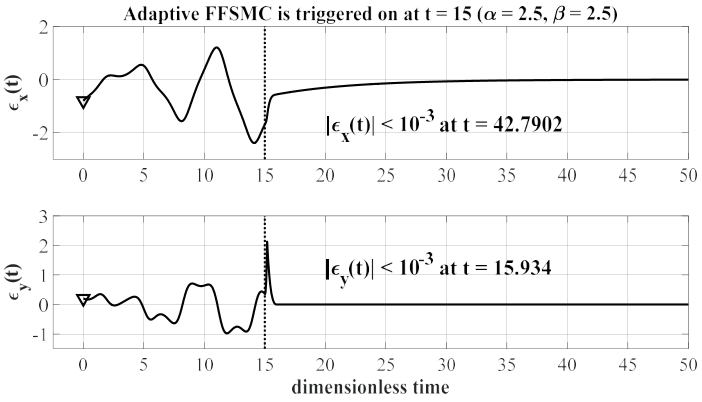

Fig. 5. Time histories of $\varepsilon_x(t)$ and $\varepsilon_y(t)$ for $\alpha = 2.5$.

The enhanced outcomes of the almost finite-time synchronization are achieved by appropriately choosing the design parameters α, β, as demonstrated by Theorem 1. For $\beta = 2.5$, Fig. 6 shows the phase portraits of $\varepsilon_x(t)$ and $\varepsilon_y(t)$ with three distinct values of α, using identical simulation parameters for coding as applied in the previous experiment. When the phase portrait starts to stay on $s(t) = 0$, it indicates that $\varepsilon_y(t)$ converges to zero more quickly for greater values of α. Subsequently, $\varepsilon_x(t)$ approaches zero. When an appropriate smaller value of α is selected, $\varepsilon_x(t)$ and $\varepsilon_y(t)$ converge almost uniformly.

Figures 7 to 9 show the results of the second numerical experiment in which $\alpha = 0.85$, $\gamma_0 = 1.5$, $\gamma_1 = 0.9$, and $\gamma_2 = 3.0$. Figures 7 and 8 depict the time responses of $\varepsilon_x(t)$, $\varepsilon_y(t)$, and $s(t)$. They show that upon the activation of the adaptive FFSMC at $t = 15$, the finite-time stability of $\varepsilon_y(t)$ is induced. At $t = 15.9141$, where $t_0 = 0.9141$, the phase portrait arrives at $s(t) = 0$, where $\varepsilon_y(t)$ is maximum. The experiment indicates the predicted time of $\varepsilon_y(t)$ to be stabilized at $t = t_s + t_0 = 16.6667$. This means that t_s of 6.5319 is the expected finite time needed to stabilize $\varepsilon_y(t)$. The theoretical value of the finite time calculated using Eq. (10) is $t_s = 6.2973$. This is essentially consistent with the expected finite time. Additionally, $\varepsilon_x(t)$ is stabilized as $\varepsilon_y(t) \to 0$, as follows.

The chatter-free continuous control signals of the suggested adaptive FFSMC method are shown in Fig. 8. For $\alpha = 0.85$, $\beta = 2.5$, the time responses of three gains, $K_1(t)$, $K_2(t)$, $K_3(t)$, are shown in Fig. 9. The outcomes indicate that all three gains eventually become constant, in line with the adaptation principles given by Eq. (14), which implies that the states $\varepsilon_x(t)$, $\varepsilon_y(t)$, and $s(t) = 0$ all tend to zero.

The phase portrait of the second numerical experiment from $t = 0$ to $t = 50$ is shown in Fig. 10. $\varepsilon_x(t)$ and $\varepsilon_y(t)$ reach $s(t) = 0$ approximately at $t = 15.91$ after the adaptive FFSMC was turned on at $t = 15$, and they subsequently remain there. Finally, the almost uniform convergence of $\varepsilon_x(t)$ and $\varepsilon_y(t)$ is demonstrated. Figure 11 shows the time responses of the states for both the diseased and healthy CASs. In Eqs. (1) and (2), the states of the two CASs deviate from one another when distinct initial conditions are selected. Both states start to synchronize when the adaptive FFSMC is activated at $t = 15$. In contrast to previous studies,[4–6,10,17,18] the chaotic synchronizations were examined using the same system parameters for both CASs. The results

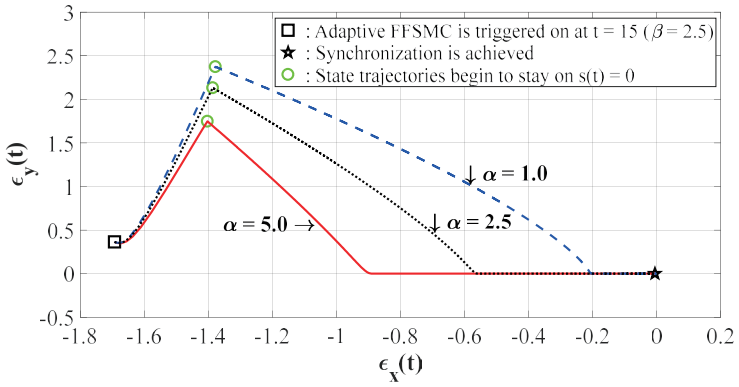

Fig. 6. (Color online) Phase portraits with different values of α.

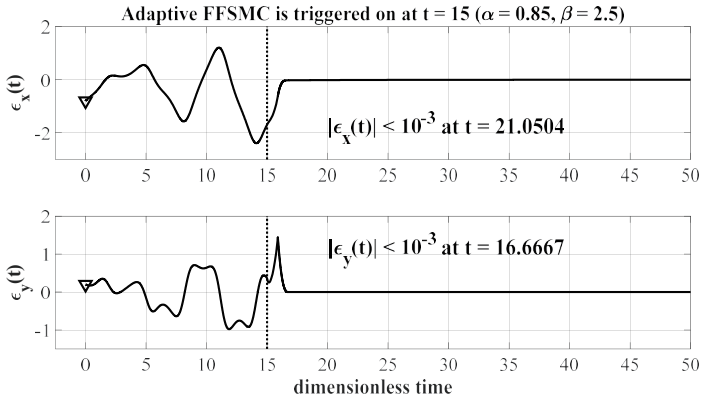

Fig. 7. Time histories of $\varepsilon_x(t)$ and $\varepsilon_y(t)$ for $\alpha = 0.85$.

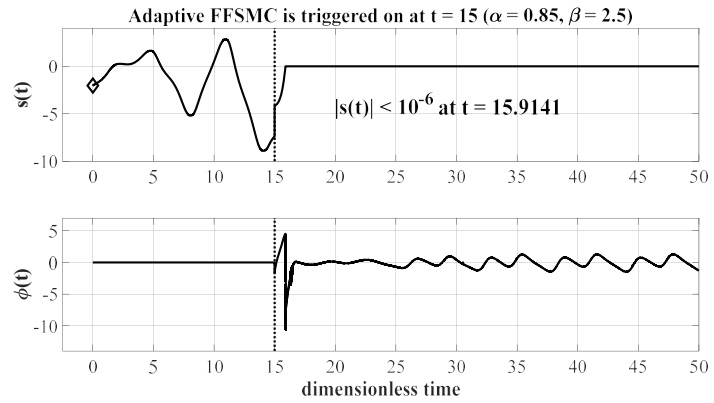

Fig. 8. Time histories of $s(t)$ and $\phi(t)$ for $\alpha = 0.85$.

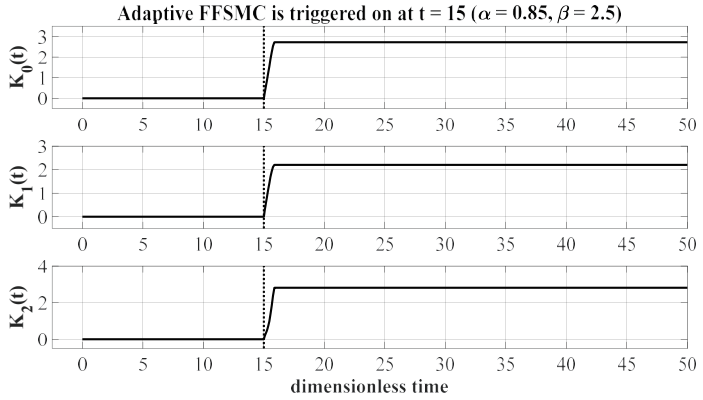

Fig. 9. Time histories of $K_i(t)$, $i = 0, 1, 2$ for $\alpha = 0.85$.

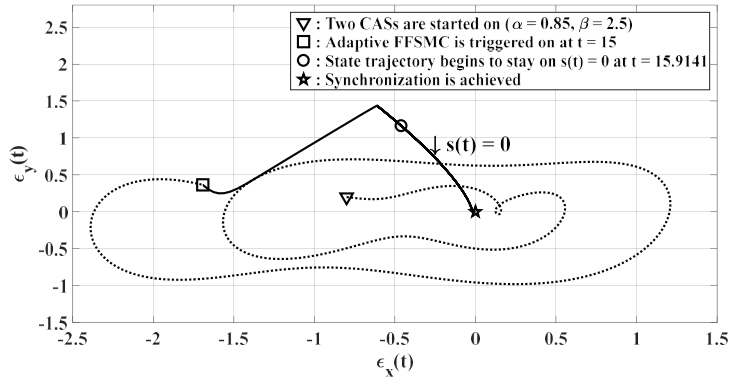

Fig. 10. Phase portrait of the second numerical experiment from $t = 0$ to $t = 50$.

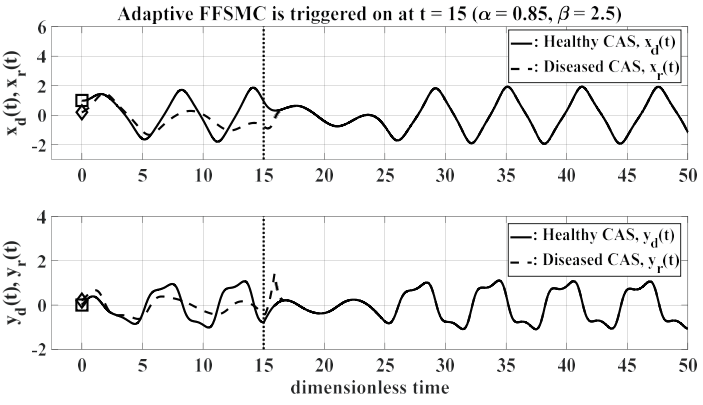

Fig. 11. Time histories of the state variables for healthy and diseased CASs.

of the current work show that even when the two CASs have distinct system parameters, synchronization can also be achieved by applying the proposed scheme.

5. Conclusions

The challenge of almost finite-time synchronization control for two CASs was overcome by adopting the proposed adaptive FFSMC. The special form of stability for the defined FFSM was described and proven. In other words, the state $\varepsilon_x(t)$ was exponentially stabilized once the state $\varepsilon_y(t)$ was first stabilized in finite time on $s(t) = 0$. The closed-loop control system was shown to be stable. Simply changing the control parameter α in the control scheme led to good performance, even when the error states were sequentially stabilized by the adaptive FFSMC approach. The validity of the existing scheme was confirmed by several numerical experiments.

Acknowledgments

This work was supported in part by Projects for the Department of Science and Technology of Fujian Province (Grants nos. 2022HZ026025, 2021-H-0060, 2021-G-02013, and 2020-H-0049) and Operational Funding of the Advanced Talents for Scientific Research (Grants nos. 19YG04 and 19YG05) of Sanming University. The authors also acknowledge the support of the School of Mechanical and Electric Engineering, Sanming University.

References

1 J. E. Skinner, A. L. Goldberger, G. Mayer-Kress, and R. E. Ideker: Nat. Biotechnol. **8** (1990) 1018. https://doi.org/10.1038/nbt1190-1018
2 S. Harshavarthini, R. Sakthivel, and F. Kong: Chaos, Solitons Fractals **134** (2020) 109683. https://doi.org/10.1016/j.chaos.2020.109683
3 Y. Shi: Discrete Dyn. Nat. Soc. **2012** (2012) 631476. https://doi.org/10.1155/2012/631476
4 C. J. Lin, S. K. Yang, and H. T. Yau: Comput. Math. Appl. **64** (2012) 988. https://doi.org/10.1016/j.camwa.2012.03.007
5 C. C. Wang and T. Y. Her: Abstr. Appl. Anal. **2013** (2013) 209718. http://dx.doi.org/10.1155/2013/209718
6 C. Y. Yeh, J. Siu, and H. T. Yau: Math. Prob. Eng. **2012** (2012) 745396. http://dx.doi.org/10.1155/2012/745396
7 K. Rajagopal, V. T. Pham, F. E. Alsaadi, F. E. Alsaadi, A. Karthikeyan, and P. Duraisamya: Eur. Phys. J. Special Top. **227** (2018) 837. https://doi.org/10.1140/epjst/e2018-700137-2
8 S. He, N. A. A. Fataf, S. Banerjee, and K. Sun: Physica A **526** (2019) 120904. https://doi.org/10.1016/j.physa.2019.04.140
9 R. Oikawa, A. Doi, M. Ishida, and B. Chakraborty: Artif. Life Rob. **28** (2023) 460. https://doi.org/10.1007/s10015-023-00854-2
10 W. S. Wu, Z. S. Zhao, J. Zhang, and L. K. Sun Nonlinear Dyn. **87** (2017) 1773. https://doi.org/10.1007/s11071-016-3151-0
11 Z. Wu, X. Zhang, and X. Zhong: IEEE Access **7** (2019) 37989. https://doi.org/10.1109/ACCESS.2019.2906770
12 U. E. Kocamaz, B. Cevher, and Y. Uyaroglu: Chaos, Solitons Fractals **105** (2017) 92. https://doi.org/10.1016/j.chaos.2017.10.008
13 Y. Z. Liu, Y. Y. Xie, Y. C. Ye, J. P. Zhang, S. J. Wang, Y. Liu, G. F. Pan, and J. L. Zhang: IEEE Photo. J. **9** (2017) 7900512. https://doi.org/10.1109/JPHOT.2016.2639291
14 C. C. Yang and C. L. Lin: Nonlinear Dyn. **69** (2012) 2089. https://doi.org/10.1007/s11071-012-0410-6
15 H. Y. Chen, K. C. Wang, H. C. Shen, and C. H. Yang: Microsyst. Technol. **27** (2021) 1107. https://doi.org/10.1007/s00542-018-4088-7
16 C. H. Yang, K. C. Wang, and L. Wu: Sens. Mater. **32** (2020) 3343. https://doi.org/10.18494/SAM.2020.2918

17 Z. S. Zhao, J. Zhang, G. Ding, and D. K. Zhang: Acta Phys. Sin. **64** (2015) 21. https://doi.org/10.7498/aps.64.210508
18 Z. S. Zhao, X. Li, J. Zhang, and Y. Pei: Int. J. Biomath. **10** (2017) 1750041. https://doi.org/10.1142/S1793524517500413
19 J. Guo and Z. S. Zhao: Mod. Phys. Lett. B **33** (2019) 1950454. https://doi.org/10.1142/S0217984919504542
20 Z. S. Zhao, Y. Du, J. Zhang, and L. Sun: Asian J. Control **21** (2018) 1. https://doi.org/10.1002/asjc.1783
21 Z. S. Zhao, F. Lv, J. Zhang, and K. Sun: Inter. J. Biomath. **12** (2019) 1950026. https://doi.org/10.1142/S1793524519500268
22 Z. Y. Zhu, Z. S. Zhao, J. Zhang, and R. K. Wang, Z. Li: Inf. Sci. **535** (2020) 225. https://doi.org/10.1016/j.ins.2020.05.056
23 X. M. Li, Z. S. Zhao, J. Zhang, and L. K. Sun: Chin. Phys. B **25** (2016) 060504. https://doi.org/10.1088/1674-1056/25/6/060504
24 H. Ding, D. Qian, S. Lee, and L. Zhu: Meas. Control **56** (2023) 1684. https://doi.org/10.1177/00202940231180842
25 G. El-khaloufi, N. Chaibi, S.B. Alaoui, and I. Boumhidi: Trans. Inst. Meas. Control (2023) (published online). https://doi.org/10.1177/01423312231182177
26 X. Yu and Z. Man: IEEE Trans. Circuits Syst. I Regul. Pap. **49** (2002) 261. https://doi.org/10.1109/81.983876